Magnetic Resonance in Medicine 54:789–797 (2005)

# Labeling Fibroblasts With Biotin-BSA-GdDTPA-FAM for Tracking of Tumor-Associated Stroma by Fluorescence and MR Imaging

D. Granot,[1] L.A. Kunz-Schughart,[2] and M. Neeman[1*]

**Fibroblasts at the tumor–host interface can differentiate into myofibroblasts and pericytes, and contribute to the guidance and stabilization of endothelial sprouts. After intravenous administration of biotin-BSA-GdDTPA-FAM in mice with subcutaneous MLS human ovarian carcinoma tumors, the distribution of the macromolecular MRI/optical contrast material was confined to blood vessels in normal tissues, while it co-registered with αSMA-positive stroma tracks within the tumor. These αSMA-positive tumor-associated myofibroblasts and pericytes showed uptake of the contrast material into intracellular granules. We evaluated the use of this contrast material for in vitro labeling of tumor fibroblasts as an approach for tracking their involvement in angiogenesis. Fluorescence microscopy demonstrated internalization of the contrast material, and MRI revealed a significant increase in the $R_1$ relaxation rate of labeled fibroblasts. $R_1$ not only remained elevated for 2 weeks in culture, it also increased with cell proliferation, indicating prolonged retention of the contrast material and subsequent intracellular processing and redistribution of the material, and thereby enhancing MR contrast. Moreover, cells that were labeled ex vivo with MR contrast material and co-inoculated with tumor cells in mice were detected in vivo by MRI. Uptake of the contrast material was suppressed by nystatin, suggesting internalization by caveolae-mediated endocytosis. This study shows that labeling of fibroblasts with biotin-BSA-GdDTPA-FAM is feasible and would allow noninvasive in vivo tracking of fibroblasts during tumor angiogenesis and vessel maturation. Magn Reson Med 54:789–797, 2005. © 2005 Wiley-Liss, Inc.**

**Key words: fibroblasts; fluorescence microscopy; angiogenesis; caveolae; MR contrast**

The integrity of epithelial tissues is highly dependent on the cross talk between the epithelium and its surrounding stroma. The stroma is comprised of fibroblasts, leucocytes, and endothelial cells that reside in an extracellular matrix (ECM) and hence are spatially separated from the epithelium by the basement membrane. When the epithelium transforms into epithelial carcinoma, the stroma inevitably changes as well (1). All solid tumors, regardless of their origin, require stroma for their progression beyond a minimal size of 1–2 mm. Tumor-associated fibroblastic stroma is often referred to as "stromal response" or desmoplasia, which is responsible for the "scirrhous" character of some carcinoma types (2–4). Indeed, the extent of the fibroblastic stromal reaction in epithelial solid tumors can account for over 90% of the total tumor mass (5). This desmoplastic reaction is characterized by pronounced alterations in the phenotype and expression profile of the associated fibroblastic cells (3). Myofibroblasts are a dominant cell population in tumor desmoplasia, and critically contribute to the abnormal distribution and composition of the extracellular matrix in carcinomas (2,3,6,7). They have been observed in the stroma of various types of epithelial tumors, such as carcinoma of the colon, breast, lung, liver, prostate, and pancreas (4,8–12), and their appearance may precede the invasive tumor stage (1). Myofibroblasts are a unique population of fibroblastic cells that possess contractile qualities through the expression of smooth muscle filaments, such as α-smooth muscle actin (SMA). Although their origin remains controversial, fibroblasts are considered to be the main progenitor cells (1,2).

Angiogenesis is a basic requirement for solid tumor growth and progression. Recent studies have suggested that fibroblastic tumor stroma, particularly myofibroblasts, essentially contribute to both the angiogenic process and cancer progression (13,14). It was suggested that fibroblasts at the tumor–host interface differentiate into myofibroblasts and then into pericyte-like cells, which are proposed to guide endothelial sprouts (15). To verify this hypothesis and to better understand the impact of fibroblasts and myofibroblasts on the development of the abnormal tumor vasculature, the interactions between endothelial cells and fibroblast cell populations in a tumor environment must be studied. Indeed, it has been shown that matrix-bound fibroblasts enhance angiogenesis as well as endothelial cell motility (16), and that co-cultures of ovarian carcinoma SKOV-3 cells with myofibroblasts facilitate the invasion of endothelial cells in 3D cultures (13). However, in order to gain deeper insight into the process of tumor angiogenesis, in vivo monitoring of fibroblast/myofibroblast–endothelial cell interactions is required.

Recent studies have suggested the use of MRI for in vivo cell tracking via paramagnetic and superparamagnetic cell labeling (17,18). One of the most promising approaches is the application of membrane-impermeable paramagnetic metal cation compounds. However, the application of these compounds has been limited, and they have been utilized mostly to monitor cell movement in embryogenesis and embryonic cell lineage analysis (19). Covalent attachment of Gd-DOTA to the HIV-Tat peptide was used for lymphocyte labeling by receptor-mediated endocytosis

[1]Department of Biological Regulation, Weizmann Institute of Science, Rehovot, Israel.

[2]Institute of Pathology, University of Regensburg, Regensburg, Germany.

Grant sponsor: NCI; Grant number: RO1 CA75334; Grant sponsors: Mark Family Foundation; Israel Science Foundation.

*Correspondence to: Michal Neeman, Department of Biological Regulation, Weizmann Institute of Science, Rehovot 76100, Israel.
E-mail: michal.neeman@weizmann.ac.il

Received 3 June 2004; revised 15 April 2005; accepted 27 April 2005.
DOI 10.1002/mrm.20628
Published online 7 September 2005 in Wiley InterScience (www.interscience.wiley.com).

(20), and the attachment of Gd-DTPA to poly-L-lysine-transferrin-DNA enabled labeling of the erythroleukemia cell line via cotransport of the contrast material with DNA during transfection (21). At present, most work in this field has focused on the detection of stem cells or cells belonging to the hematopoietic system. The goal of the present study was to establish and verify a technique to label fibroblasts in vitro, and to characterize the uptake mechanism, retention, and MR visibility of the contrast material. This work provides the basis for future in vivo MR monitoring, with the intention to detect the interaction of fibroblasts with the vessel wall during tumor angiogenesis and vascular remodeling.

In this study we show that fibroblasts can be efficiently labeled ex vivo with biotin-BSA-GdDTPA without loss of cell viability, thus providing MR-detectable contrast both in vitro and in vivo. Additionally, in a xenograft model of human fibroblasts and human ovarian cancer cells, after intravenous administration of biotin-BSA-GdDTPA, immunohistochemical staining detected the contrast material intracellularly in myofibroblasts. This model is of particular interest since in a previous study we reported that the exit of implanted human MLS ovarian carcinoma spheroids from dormancy correlated with the infiltration of α-SMA-positive (myo)fibroblasts into the tumor mass, suggesting a critical role for these cells in the initiation of tumor progression (14). Moreover, we recently showed that these stroma myofibroblasts contributed to vascular stabilization and maturation in ovarian tumors by the expression of angiopoietin-1 (22).

## MATERIALS AND METHODS

### Contrast Material

Biotin-BSA-GdDTPA-FAM was synthesized as previously described (23). The protein concentration was determined by ultraviolet absorption at 280 nm against a standard concentration of BSA. The degree of fluorescence of 5(6)-carboxyfluorescein, succinimidyl ester (FAM; Molecular Probes Inc., Eugene, OR, USA) labeling was determined according to the manufacturer's protocol (two to four FAM molecules per BSA). The number of biotin groups bound to BSA was measured using HABA/avidin reagent (Sigma Chemical Co., St. Louis, MO, USA; one to two biotin moieties per BSA molecule). Gadolinium (Gd) was measured by an inductively coupled plasma-atomic emission spectrometer (ICP-AES, Optima 3300; Perkin Elmer, Norwalk, CT, USA; 27 GdDTPA per BSA).

The longitudinal proton relaxation rate ($R_1$) was determined at room temperature on a 4.7 T Bruker Biospec (Karlsruhe, Germany) spectrometer for a range of concentrations of the contrast material. Longitudinal relaxation rates were measured using spin-echo images (flip angle = 90°) with 10 TRs (100–2000 ms) and TE = 10 ms for each concentration. The relaxivity of the contrast material was calculated as previously reported (23) and was found to be 186 $mM^{-1}s^{-1}$ (6.8 $s^{-1}$ per mM GdDTPA).

### Cell Culture

Primary fibroblasts were obtained from normal skin (N1), normal breast (PFN2), and ductal breast carcinoma biopsies (PF40T: from a highly differentiated G1 breast tumor; PF42T: from a poorly differentiated invasive G3 breast tumor), and were characterized and processed as previously described (24). For the present experiments, fibroblasts were cultured from frozen stocks in Dulbecco's Modified Eagle's Medium (DMEM) with a cumulative population doubling (CPD) of <40. Assays were performed using primary fibroblasts of passages 3–7. A cos-7 cell line was cultured in DMEM medium. MLS, a human ovarian epithelial carcinoma cell line, was cultured in α minimal essential medium (MEM). All media were supplemented with 10% FCS, 100 U/ml penicillin, 0.1 mg/ml streptomycin, 0.06 mg/ml amphotericin B, and 2 mM L-glutamine. The media and serum were purchased from Biological Industries (Beit Haemek, Israel).

### Ex Vivo Cell Labeling

The fibroblasts labeled for MRI measurements were grown to confluence in 6-cm culture plates. The fibroblasts were incubated on a rotating board in fresh culture medium supplemented with 10 mg/ml biotin-BSA-GdDTPA. After 48 hr of incubation, labeling was terminated by removal of the medium and four washes with serum free medium.

Retention of the contrast material was assayed using labeled cells (passages 6 and 7), which were subsequently washed and cultured in fresh medium. In some cases, cells were harvested with trypsin-EDTA after they were labeled, and then washed and replated in fresh medium. After an additional culture period of up to 2 weeks, the cells were analyzed by MRI. The role of caveolae in biotin-BSA-GdDTPA uptake into the fibroblasts was assessed by the addition of nystatin (50 μM; Sigma) to the labeling media. The correlation between proliferation and relaxivity of the contrast material was determined using the cos-7 cell line. The cos-7 cells, which were grown to subconfluence in a 10-cm dish, were labeled with 10 mg/ml biotin-BSA-GdDTPA for 24 hr. At each subsequent time point $1 \times 10^6$ cells in log phase were taken for MRI analysis, and $2 \times 10^6$ were seeded for further culturing in 10-cm plates.

Intracellular gadolinium (Gd) content in labeled cos-7 cells was determined by ICP-AES. At each time point, $3 \times 10^6$ labeled cos-7 cells were treated with nitric acid to remove all organic compounds prior to Gd measurement. The relaxivity of the intracellular contrast material was determined according to:

$$R_{IC} = \Delta R_1/[Gd] \quad [1]$$

where $R_{IC}$ is the intracellular relaxivity, $\Delta R_1$ is the change in longitudinal relaxation rate as measured by MRI, and [Gd] is the intracellular concentration in pmol/cell as measured by ICP-AES.

Fluorescence imaging of labeled cells was performed with cells grown to subconfluence on 12-mm coverslips. The cells were labeled with the fluorescent (FAM) conjugated contrast material for 48 hr as described above. They were then washed with serum-free medium and fixed for 20 min in 3% paraformaldehyde, and the nuclei were stained (5 μg/ml propidium iodide (PI); Sigma). The contrast material and PI were detected by fluorescence confo-

cal microscopy (Axiovert 100; Zeiss, Goettingen, Germany).

Cell survival was determined for cells cultured in 96-well plates by neutral red accumulation as previously described (25). The mean net optical density (mean ± SEM) was computed and found to be 570 nm after the assay blanks were subtracted.

### In Vitro MRI Measurements of Ex Vivo Labeled Cells

NMR microscopy measurements were performed on a 400 MHz (9.4 Tesla) vertical wide-bore DMX spectrometer equipped with a microimaging attachment with a 5-mm Helmholtz radiofrequency (RF) coil (Bruker). Labeled and control cells (primary human fibroblasts, $3 \times 10^5$ cells; and cos-7 cell line, $1 \times 10^6$ cells) were washed four times in serum-free medium, harvested with trypsin-EDTA, and suspended in 1% low-gelling-temperature agarose (Sigma; 200 μl/500 μl for primary human fibroblasts and cos-7 cells, respectively), in 5-mm (o.d.) NMR tubes (Wilmad Glass Company, Buena, NJ, USA).

### $R_1$ Measurements

Spin-echo images were acquired with different TRs (100–2000 ms); TE = 8.8 ms; 128 × 128 pixels; two averages; slice thickness = 1 mm; FOV = 1.5 cm × 0.6 cm; in-plane resolution = 117 × 47 μm; and spectral width (SW) = 50000 Hz.

The MRI data were analyzed with the use of Matlab computing software (The Mathworks Inc., Natick, MA, USA). Images acquired with 10 different TR values were used to generate $R_1$ maps and calculate average $R_1$ values in selected regions of interest (ROIs), by nonlinear least-square pixel-by-pixel fitting to a single exponent. The mean $\Delta R_1$ was calculated from the differences in $R_1$ between labeled and unlabeled cells (mean values ± SEM are reported). Student's *t*-test (paired, one-tailed) was used for statistical analysis to compare control and labeled groups.

### Animal Experiments

The animal experiments were approved by the Weizmann Institutional Animal Care and Use Committee. CD1-nude mice (female, $N = 4$, 6–10 weeks old, body weight = 28–30 g) were studied 14–20 days after subcutaneous co-inoculation in the hind limb of MLS ovarian carcinoma cells and PF42T fibroblasts derived from a desmoplastic, poorly differentiated breast tumor ($1 \times 10^6$ and $2.5 \times 10^5$ cells/mouse, respectively). The mice were anesthetized by intraperitoneal injection of 75 mg/kg ketamine (Fort Dodge Animal Health, Fort Dodge, IA, USA) and 3 mg/kg xylazin (XYL-M2, V.M.D, Arendox, Belgium), followed by additional subcutaneous injection of half a dose. The tail vein was catheterized and biotin-BSA-GdDTPA was injected intravenously (12 mg/mouse in 0.2 ml PBS). The mice were killed approximately 30 min after administration of the contrast material. Tumor samples were removed and fixed in Carnoy's solution (6:3:1 ethanol/chloroform/acetic acid).

### Immunohistochemistry

Fixed tumor samples were embedded in paraffin blocks and serially sectioned (4 μm). Following deparaffinization with xylene and rehydration in ethanol (100%, 95%, 70%, and double distilled water (DDW), the sections were blocked and incubated with monoclonal anti-α-SMA antibody (alkaline phosphatase (AP) conjugated, 1:30; Sigma). Biotinylated contrast material was detected by incubation with avidin-FITC (1:40; Sigma). The nuclei were counterstained with Hoechst reagent (1:1000 in PBS; Molecular Probes), and the sections were sealed with antifade reagent (Molecular Probes).

### In Vivo MRI Measurements of Ex Vivo Labeled Cells

Cos-7 cells grown to subconfluence in a 15-cm culture dish were incubated with 10 mg/ml biotin-BSA-GdDTPA for 48 hr. Following washes, labeled/control cos-7 cells ($5 \times 10^6$) were co-inoculated subcutaneously with an equivalent number of MLS cells into the hind limb of CD1-nude mice (female, $N = 4$ for each group, 6–10 weeks old, body weight = 28–30 g).

MRI experiments were performed on a horizontal 4.7 T Bruker Biospec spectrometer using an actively RF-decoupled 2-cm surface coil stabilized in a Perspex board, and a whole-body birdcage transmission coil. The mice were studied 1 day after co-inoculation with the tumor MLS cells and cos-7 labeled/control cells. Anesthetized mice were placed with the tumor region in the center of the surface coil. A series of $T_1$-weighted 3D gradient-echo (GE) images, with pulse flip angles of 5°, 15°, 30°, 50°, and 70° were acquired to determine the $R_1$ values. The acquisition parameters were as follows: TR = 10 ms; TE = 3.561 ms; two averages; spectral width 50,000 Hz; FOV = 6 × 6 × 3 cm, 128 × 128 × 64 pixels, resulting in a voxel resolution of 470 × 470 × 470 μm; and total acquisition time per frame = 163 s.

3D-GE data sets were used to generate $R_1$ maps and calculate the average $R_1$ values in selected ROIs by nonlinear best fit to:

$$I = \frac{M_0 \sin\alpha \ (1 - e^{-TR*R1})}{1 - \cos\alpha * e^{-TR*R1}} \quad [2]$$

where $I$ is the signal intensity as a function of the pulse flip angle; TR = 10 ms; and the pre-exponent term, $M_0$, includes the spin density and the $T_2$ relaxation. Student's *t*-test (two-tailed, equal variance) was used for statistical analysis of the significance of change in the relaxation rate between control and labeled tumors.

## RESULTS

### In Vivo Labeling of Tumor Stroma

Tumor xenografts were initiated from a human ovarian carcinoma cell line (MLS) co-inoculated with human tumor-derived fibroblasts (PF42T). The mice were killed approximately 30 min after intravenous administration of biotin-BSA-GdDTPA. The distribution of the biotinylated contrast material in the tumor mass was detected by avidin-FITC staining of thin histological sections. During the time interval between intravenous administration of the contrast material and sacrifice of the mice, contrast material leaked from blood vessels into the tissue at sites of

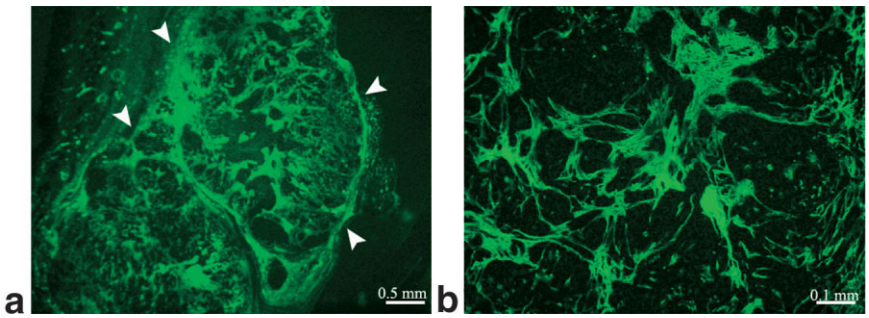


FIG. 1. Distribution of the contrast material in MLS tumors. Fluorescence microscopy of representative tumors initiated by co-inoculation of MLS cells and PF42T fibroblasts. Biotin-BSA-GdDTPA was administered intravenously into the tail vein of a tumor-bearing mouse (16 days after implantation, 30 min prior to tumor retrieval). The distribution of biotin-BSA-GdDTPA was detected by staining with avidin-FITC. Tumor borders are illustrated by arrowheads (**a**).

hyperpermeability (Fig. 1). Low-magnification views (e.g., Fig. 1a) revealed that the contrast material was localized at the tumor rim delineating the borders of the tumor (Fig. 1; arrowheads) with channels extending into the tumor inner mass. Images with a higher magnification (Fig. 1b) showed that the contrast material was not chaotically scattered, but rather reflected a pattern associated with specific types of stromal cell tracks.

Since myofibroblasts are the most abundant cell type in the stroma of epithelial carcinomas, we double stained the tumor specimens with avidin-FITC and anti-α- SMA. The results not only verified the association between contrast material and myofibroblasts, they also confirmed that contrast material remained confined to areas of α-SMA-positive myofibroblasts, without penetrating the "nodules" of tumor cells (Fig. 2). Some contrast material was detected within intracellular granules in these myofibroblasts (arrowheads). Contrast material was found localized in α-SMA-positive cells that surrounded a large blood vessel (Fig. 2, tumor #1 (yellow)), as well as in α-SMA-negative tracks that were surrounded by α-SMA-positive cells. Therefore, we evaluated the potential of exploiting this uptake to develop a new approach for ex vivo labeling of tumor-associated fibroblasts and myofibroblasts.

## Ex Vivo Labeling of Fibroblasts With Biotin-BSA-GdDTPA-FAM

In view of the importance of fibroblasts and myofibroblasts in regulating tumor perfusion, and the intracellular uptake of contrast material into these cells, we assessed the use of biotin-BSA-GdDTPA-FAM for ex vivo prelabeling of fibro-

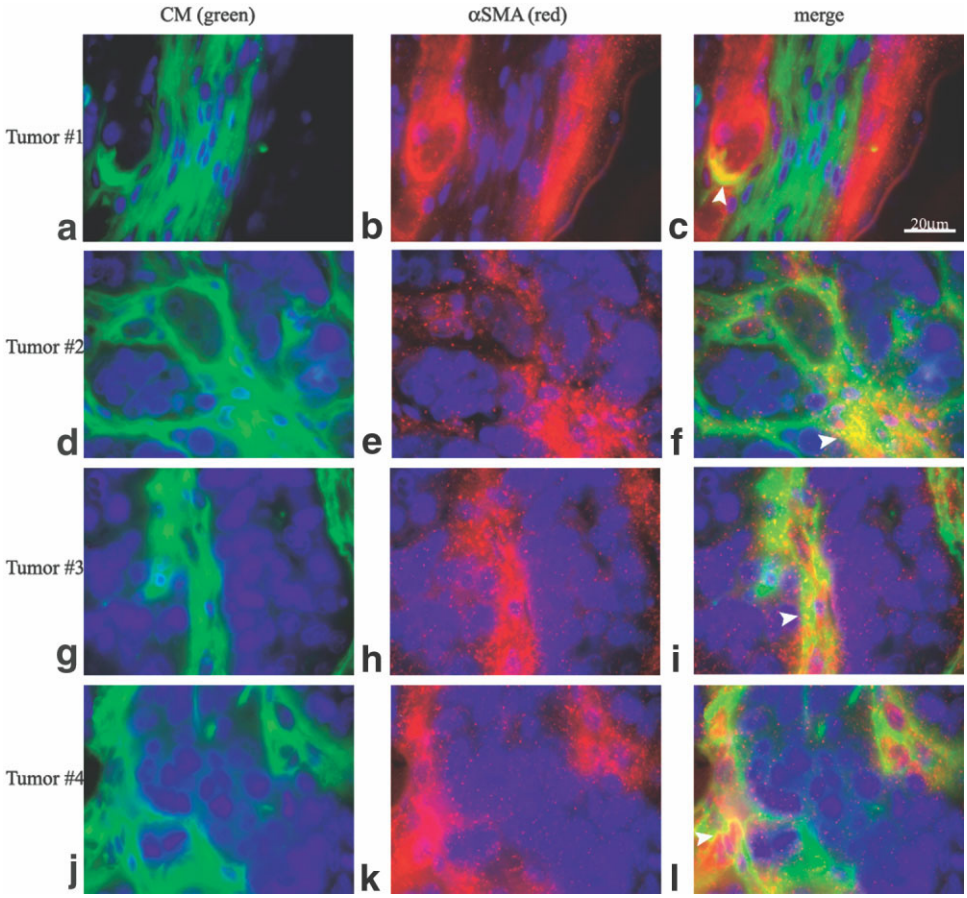


FIG. 2. Internalization of contrast material into myofibroblasts in vivo. Immunohistochemical fluorescence microscopy of representative images acquired from four individual tumors initiated by co-inoculation of MLS cells and PF42T fibroblasts. Biotinylated contrast material (avidin-FITC (**a**, **d**, **g**, and **j**; green)) was intravenously administered into the tail vein of tumor-bearing mice (16 days after implantation, 30 min prior to tumor retrieval). α-SMA staining of pericytes, vascular smooth muscle cells, and myofibroblasts (**b**, **e**, **h**, and **k**; red); merged images (**c**, **f**, **i**, and **l**); and nuclear staining (a–f; blue) are shown. Arrowheads indicate intracellular uptake.

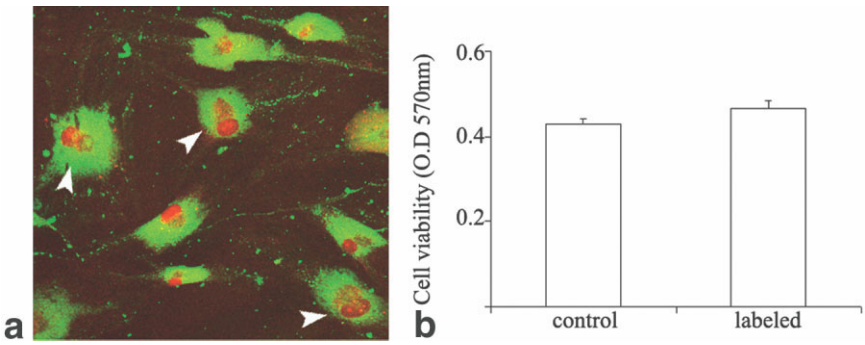


FIG. 3. Viability of fibroblasts after ex vivo labeling. **a:** Confocal microscopy of PFN2 fibroblasts double labeled with biotin-BSA-GdDTPA-FAM (48 hr, 10 mg/ml) and propidium iodide (nuclear staining). Arrowheads indicate proliferating cells. **b:** Neutral red incorporation was used to measure cell viability in control unlabeled cells and in labeled cells. Optical density was measured at 570 nm (mean ± SEM, $N = 9$, $P = 0.12$, *t*-test, unpaired, two-tailed).

blasts. Tumor-derived and normal human breast fibroblasts were incubated with biotin-BSA-GdDTPA-FAM (48 hr, 10 mg/ml), followed by extensive washes to remove excess contrast material. Cells that were labeled with the fluorescent tagged contrast material were fixed and counterstained with PI (5μg/ml) to identify all cell nuclei. In contrast to unlabeled fibroblasts, the cytoplasm of labeled PFN2 normal breast fibroblasts showed high fluorescence (green), demonstrating internalization of the fluorescein-labeled contrast material (Fig. 3a). After 48 hr of incubation, 100% of the cells were fluorescently labeled. Thus, the contrast material was internalized into the cytoplasm of all cells, revealing the high efficiency of this labeling procedure.

### Cells Remain Viable After Labeling

The viability of cells treated with biotin-BSA-GdDTPA was evaluated after 48 hr of labeling (10 mg/ml) by means of the neutral red viability assay (Fig. 3b). The number of viable cells in labeled fibroblasts did not differ from that in an unlabeled control. Hence the cell viability was not affected by the labeling procedure. In addition, confocal microscopy revealed cells that were in the process of cell division (Fig. 3a, arrowheads).

### Labeled Cells Are MR Visible

To determine whether the intracellular contrast material was detectable by MRI, we measured the $R_1$ relaxation rates of control and labeled cells (10 mg/ml biotin-BSA-GdDTPA, 48 hr). MR images of fibroblasts suspended in agarose ($3 \times 10^5$ cells/0.2 ml) were obtained to derive $R_1$ relaxation maps (Fig. 4a and b) and calculate the average $R_1$ in selected ROIs (Fig. 4c and d). Data analysis revealed a significant increase in $R_1$ relaxation rates of labeled cells. In detail, the $R_1$ values of labeled fibroblasts derived from normal skin, normal breast, or breast tumor (N1, PFN2, and PF40T/PF42T, respectively) were compared with the $R_1$ values of corresponding unlabeled control fibroblasts. In all cases, incubation with biotin-BSA-GdDTPA significantly elevated the $R_1$ value, resulting in positive $\Delta R_1$ (Fig. 4d; $\Delta R_1 = R_1(\text{labeled}) - R_1(\text{unlabeled}) > 0$ for all fibroblast types; $P < 0.03$). The increase in the $R_1$ relaxation rate is in accord with both the intracellular uptake and the MR visibility of the intracellular contrast material.

### Caveolae-Mediated Internalization of Biotin-BSA-GdDTPA

Most cells internalize albumin via endo- or pinocytosis in a process that may be mediated by caveolae (26). The mechanism of contrast material internalization into fibroblasts was evaluated by the addition of nystatin to the labeling media. Nystatin, a general inhibitor of caveolae-mediated endocytosis, is known to precipitate cholesterol in the plasma membrane of the cell, thereby disrupting caveolae function (27). Fibroblasts were labeled with biotin-BSA-GdDTPA (48 hr, 10 mg/ml) with or without the addition of nystatin (50 μM). MRI measurements of $R_1$

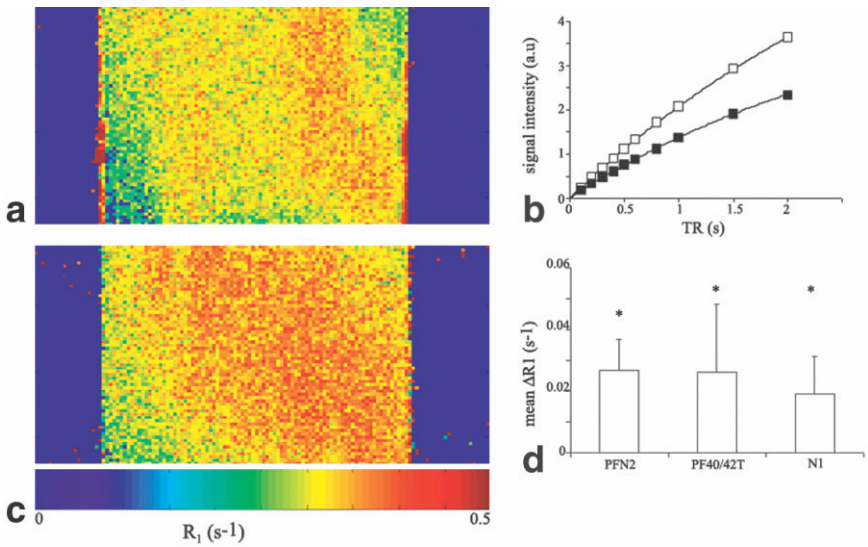


FIG. 4. Detectable increase in the $R_1$ relaxation rate of fibroblasts labeled with biotin-BSA-GdDTPA. $T_1$-weighted images of control and labeled cells were acquired on a 400 MHz spectrometer. Representative $R_1$ maps of (**a**) unlabeled cells and (**c**) cells labeled with biotin-BSA-GdDTPA contrast material (48 hr, 10 mg/ml). **b:** Nonlinear single exponential fittings of signal intensity as a function of TR, used to derive $R_1$ for unlabeled (close squares) and labeled (open squares) cells. **d:** MRI detection of the change in $R_1$ ($\Delta R_1 = R_1(\text{labeled}) - R_1(\text{unlabeled})$, obtained from ROI analysis) of fibroblasts labeled with biotin-BSA-GdDTPA compared with that of unlabeled cells (PFN2, $N = 4$; PF40/42T, $N = 3$; N1, $N = 2$; * significant change in $R_1$ of labeled vs. unlabeled cells; $P < 0.03$, *t*-test, paired, one-tailed).

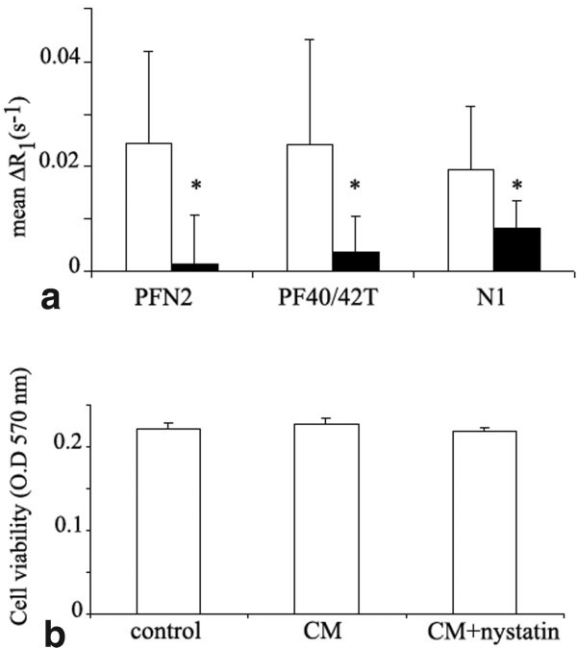


FIG. 5. Nystatin inhibits internalization of biotin-BSA-GdDTPA into fibroblasts. **a:** Various primary fibroblasts were labeled with biotin-BSA-GdDTPA (48 hr, 10 mg/ml) in the presence (close bars) or absence (open bars) of the caveolae inhibitor nystatin (50 μM; PFN2, $N = 3$; PF40/42T, $N = 2$; N1, $N = 2$; $^*P = 0.006$ for nystatin effect *t*-test, paired, one-tailed). **b:** Neutral red incorporation was used to measure cell viability in PFN2 cells after incubation with CM and nystatin. Optical density was measured at 570 nm (mean ± SEM, $N = 12$, $P > 0.5$, *t*-test, unpaired, two-tailed).

showed that uptake of biotin-BSA-GdDTPA was significantly suppressed by the presence of nystatin in the labeling media (Fig. 5a, $P = 0.006$). In all fibroblast types, the elevation in $R_1$ was considerably restrained by nystatin, and in PFN2 fibroblasts $\Delta R_1$ was almost abolished. Cells that were grown in the presence of nystatin remained intact, as visualized by microscopy prior to the MRI assays, and viable, as demonstrated by a neutral red viability assay performed with nystatin in the labeling medium (Fig. 5b). The inhibition of labeling of cells by nystatin emphasizes the role of specific endocytosis and caveolae in the internalization of biotin-BSA-GdDTPA into fibroblasts ex vivo.

### MR Signal Is Retained in Labeled Cells for at Least 2 Weeks in Culture

For in vivo follow-up of prelabeled cells, the contrast material should remain detectable in the cells or their progeny over a sufficient period. Therefore, we assessed the retention of biotin-BSA-GdDTPA in both normal PFN2 and tumor-derived PF42T fibroblasts, as well as the ability of labeled cells to readhere to the surface of the culture plate. After incubation with biotin-BSA-GdDTPA (48 hr, 10 mg/ml) and extensive washes, the cells were either incubated in fresh medium for an additional culturing period (up to 2 weeks), or harvested with trypsin-EDTA before they were replated in fresh medium for further culturing. After 2 weeks in culture, the cells were harvested, counted, and suspended in agarose ($3 \times 10^5$ cells/0.2 ml), and $R_1$ was assessed (Fig. 6a). MRI measurements showed that even after 2 weeks of subsequent culturing, biotin-BSA-GdDTPA labeled cells maintained significantly higher $R_1$ values than unlabeled control cells ($P < 0.01$). In addition, the ability of the cells to readhere to the culture plates was not affected by labeling treatment, and, vice versa, harvesting and replating did not affect the $R_1$ values of the labeled cells. Thus, MR-detectable contrast material was retained in the cells for at least 2 weeks.

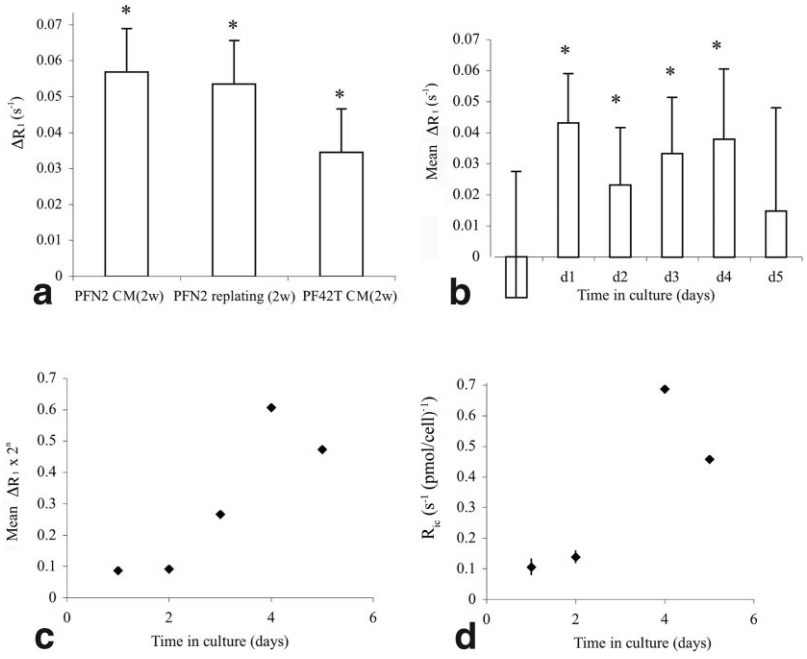


FIG. 6. Prolonged intracellular retention and enhanced visibility of the contrast material during cell proliferation. **a:** PFN2 and PF42T fibroblasts were labeled with biotin-BSA-GdDTPA (48 hr, 10 mg/ml) and incubated in fresh medium for up to 2 weeks (PFN2 2w; PF42T 2w), or harvested prior to additional incubation (PFN2 2w replating). $\Delta R_1$ was measured after 2 weeks of further culturing ($^*P < 0.01$ for labeling retention; *t*-test, paired, one-tailed). **b:** Cos-7 cells were labeled with the contrast material (24 hr, 10 mg/ml). $\Delta R_1$ was measured daily, each time for new $1 \times 10^6$ cells harvested from log phase monolayer culture ($^*P < 0.03$ for labeling retention; $\Delta R_1 > 0$ relative to unlabeled cells; *t*-test, paired, one-tailed). **c:** Effective relaxivity ($R_{ef}$) of the contrast material was derived from $\Delta R_1$ (b) according to the equation $R_{ef} \propto \Delta R_1 \times 2^n$ (where n is the number of cell divisions). **d:** Intracellular relaxivity ($R_{IC}$) of the contrast material was calculated according to the equation $R_{IC} = \Delta R_1$/[Gd] (where [Gd] is the intracellular concentration in pmol/cell as measured by ICP-AES). Daily concentrations of [Gd] were determined from average measurements of six individual labeling repetitions (mean ± SEM).

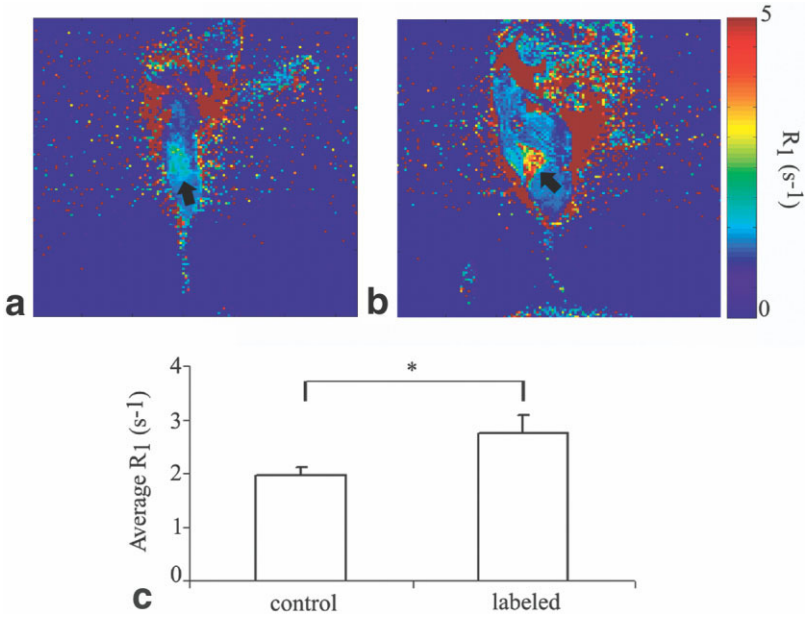


FIG. 7. In vivo detection of ex vivo labeled fibroblasts. $T_1$-weighted 3D-GE images acquired on a horizontal 4.7 T Biospec spectrometer. Representative $R_1$ maps of tumors initiated from MLS cells co-inoculated with (**a**) unlabeled cos-7 cells and (**b**) cells labeled with biotin-BSA-GdDTPA contrast material (48 hr, 10 mg/ml). Arrows indicate tumor region. **c:** Average $R_1$ values obtained from ROI analysis of the tumor regions initiated from MLS cells co-inoculated with cos-7 cells, untreated ($N$ = 4) or labeled with biotin-BSA-GdDTPA ($N$ = 4). (*Significant change in $R_1$ of labeled vs. unlabeled tumors; $P$ = 0.01, $t$-test, unpaired, two-tailed).

### Relaxivity of the Intracellular Contrast Material Increases With Cell Proliferation

Unexpectedly, further enhancement of the labeling contrast was observed with time after labeling, despite the dilution of label by cell proliferation (the same number of cells was taken for each measurement; Figs. 4d and 6a). Thus, after additional incubation of the cells, the observed $\Delta R_1$ was greater than the $\Delta R_1$ measured immediately after labeling. To evaluate the impact of cell proliferation on the relaxivity of the contrast material, we conducted additional experiments using the cos-7 cell line. As opposed to primary fibroblasts, which are characterized by a very moderate proliferation rate and undergo senescence after a few cell divisions, cos-7 cells divide every 24 hr. After incubation with biotin-BSA-GdDTPA (24 hr, 10 mg/ml), excess contrast material was removed by four washes. After harvesting with trypsin, a fraction of the cells were immediately analyzed by MRI ($1 \times 10^6$ cells), while the remaining cells were replated for further divisions ($2 \times 10^6$ cells/10 cm plate). $R_1$ was determined on a daily basis for log phase cells, suspended in agarose (each time $1 \times 10^6$ cells/0.5 ml agarose). The results (Fig. 6b) show that significant level of $\Delta R_1$ persists throughout the four initial cell cycles. Hence, although cells proliferated, resulting in a twofold dilution of the contrast material every 24 hr, no corresponding decrease in $\Delta R_1$ was observed. The effective relaxivity of the intracellular contrast material ($R_{ef}$), which we derived by assuming a 24-hr doubling time ($R_{ef} = \Delta R_1 \times 2^n$), highlights the increased visibility of Gd in the labeled cells after a few cell divisions (Fig. 6c). Moreover, the calculation of the intracellular relaxivity ($R_{IC} = \Delta R_1$/[Gd]), in which the intracellular concentration of gadolinium ([Gd] in pmol/cell) was determined by ICP-AES, confirmed enhancement of intracellular relaxivity of the contrast material (Fig. 6).

### In Vivo Detection of Ex Vivo Labeled Fibroblasts

The in vitro results encouraged us to proceed with an in vivo assessment of the visibility of the labeled cells. MLS tumors were generated in CD-1 nude mice by co-inoculation with cos-7 cells, either prelabeled ex vivo (48 hr, 10 mg/ml b-BSA-GdDTPA; $N$ = 4), or untreated control cells ($N$ = 4). A day after inoculation, the labeled tumors showed clearly and significantly higher $R_1$ values compared to control tumors (Fig. 7). Thus, ex vivo labeled cos-7 cells are easily detectable in vivo by MRI.

## DISCUSSION

MRI is emerging as a powerful tool for cell tracking via paramagnetic and superparamagnetic cell labeling (27–34). Superparamagnetic iron oxide (SPIO) particles have been used both clinically (28) and in research studies of various biological processes, such as the detection of stem cells, tumor cells, and tumor-associated macrophages; migration and homing of stem cells to bone marrow, lymphocytes in the liver, spleen, and pancreas; and detection of T-cells and THP-1 phagocytes (29–33). More recently, ultrasmall SPIO (USPIO) particles were used for lymphography and detection of T-cells in rat testicles and macrophages within the central nervous system (34,35). However, paramagnetic metal cation compounds, which are membrane impermeable, were mostly utilized by microinjection, by covalent attachment to specific peptides, or in conjugation with transfection agents (19,20).

In this study we have demonstrated that the administration of multimodal triple-labeled albumin-based contrast material results in its spontaneous internalization into tumor associated myofibroblasts, where it appears to be localized in intracellular granules. This was established both ex vivo by incubation of cells with the contrast material, and in vivo by intravenous administration of the contrast material to tumor-bearing mice. Ex vivo, incubation of human fibroblasts derived from skin, normal breast, and breast tumor tissues with the fluorescent-conjugated contrast material confirmed the uptake of biotin-BSA-Gd-DTPA-FAM into cytoplasmic granules (presumably lysosomes). The physiological effects of labeling were evaluated in order to verify that uptake of the contrast material

does not impact cellular function. The parameters tested included the ability of cells to adhere to the surface of the culture plate, cell membrane integrity (viability), and cell division. Dividing cells were visualized by confocal microscopy, which revealed multiple labeled cells in mitosis. Similarly, the adhesion of cells after trypsinization, and the number of viable cells after continuous culture were unaffected by the labeling procedure and uptake, indicating an unaltered balance in cell death and proliferation characteristics of the fibroblast cultures.

Internalization of the contrast material was detectable by both fluorescence microscopy and MRI. The $R_1$ relaxation rates of the three primary human fibroblast types were significantly elevated after incubation with the contrast material. Thus, not only was the contrast material internalized into the cells, it was also MR visible. Uptake and internalization of the contrast material, as manifested by the elevated $R_1$ relaxation rate, was effectively suppressed by treating the cells with nystatin, a cholesterol-sequestering agent that has been suggested as a specific inhibitor of caveolae-mediated endocytosis. These results implicate caveolae in mediating endocytosis, and accumulation of the contrast material in fibroblasts. The role of caveolae in endocytosis is further supported by the preliminary finding that all three fibroblast types assessed in this study expressed caveolin-1, the most abundant component of caveolae (data not shown).

We demonstrated the retention of labeling in fibroblasts by culturing cells for up to 2 weeks following the labeling process. The $R_1$ relaxation rates of the labeled cells remained considerably elevated relative to the unlabeled control cells. Moreover, relaxation rates increased with time in culture. Following proliferation, despite dilution of the contrast material, the changes in $R_1$ were similar throughout the first four cell cycles for the same number of suspended cells. Derivation of the effective relaxivity of the contrast material showed increased visibility of Gd during the first four cell cycles. This was further established by the calculation of intracellular relaxivity from the change in $R_1$ and intracellular Gd concentration. Thus, we conclude that the relaxivity of the contrast material increased with cell proliferation. This finding is consistent with initial internalization of the contrast material into intracellular granules, which was previously demonstrated to limit its detection by MRI (36,37). Cell proliferation along with catabolism of albumin through lysosomal degradation would result in redistribution of the contrast material in intracellular compartments, and hence increase its effect on water relaxation. The early sequestration of the contrast material in granules, together with the finding that relaxivity may be enhanced with proliferation, should improve sensitivity for in vivo detection of fibroblast proliferation in tumors, and furthermore suggests that it may be possible to determine the number of cell divisions from the relative changes in $R_1$ and $R_2$ relaxation rates. In this regard, our in vivo study demonstrates that prelabeled fibroblasts are MR visible. Remarkably, but in accord with the higher cell density, the contrast detected from labeled cells in vivo was greater than that obtained in vitro.

In summary, triple-labeled albumin was developed in this study for the detection of tumor-associated fibroblasts by MRI and optical imaging. Uptake of the contrast material via caveolae-mediated endocytosis into intracellular granules resulted in a significant enhancement of the $R_1$ relaxation rate. Together with the in vivo visibility of labeled cells, these results provide the basis for future use of MRI to analyze the recruitment of fibroblasts prelabeled with biotin-BSA-GdDTPA-FAM during tumor progression. Tracking fibroblasts in tumor models could provide insights into how fibroblasts differentiate in tumors and help support tumor angiogenesis and vessel maturation. Indeed, although in vitro coculture models of endothelial cells and myofibroblasts suggested their fundamental impact on tumor angiogenesis (1,13,15), the interactions that occur in vivo are still not well understood, and the role of fibroblasts in vessel formation and maturation is still ambiguous. It is well known, however, that both endothelial cells and fibroblasts are located in close association in many epithelial tumors, i.e., in those expressing a desmoplastic response. We recently reported the critical role of myofibroblasts in the initiation of growth of dormant MLS ovarian epithelial tumor xenografts (14), and in the stabilization and maturation of the tumor vasculature (22). These tumor xenografts are not only massively infiltrated by αSMA-positive stromal cells (myofibroblasts/pericytes), they are also characterized by a moderate and nonleaky vasculature. Fibroblasts prelabeled with biotin-BSA-GdDTPA-FAM in combination with MRI and the xenograft model could provide a fundamental tool for elucidating the role of fibroblasts in tumor angiogenesis.

## REFERENCES


1. De Wever O, Mareel M. Role of tissue stroma in cancer cell invasion. J Pathol 2003;200:429–447.
2. Elenbaas B, Weinberg RA. Heterotypic signaling between epithelial tumor cells and fibroblasts in carcinoma formation. Exp Cell Res 2001; 264:169–184.
3. Kunz-Schughart LA, Knuechel R. Tumor-associated fibroblasts (part II): functional impact on tumor tissue. Histol Histopathol 2002;17:623–637.
4. Kunz-Schughart LA, Knuechel R. Tumor-associated fibroblasts (part I): active stromal participants in tumor development and progression? Histol Histopathol 2002;17:599–621.
5. Dvorak HF. Tumors: wounds that do not heal. Similarities between tumor stroma generation and wound healing. N Engl J Med 1986;315: 1650–1659.
6. Ronnov-Jessen L, Petersen OW, Bissell MJ. Cellular changes involved in conversion of normal to malignant breast: importance of the stromal reaction. Physiol Rev 1996;76:69–125.
7. Sappino AP, Skalli O, Jackson B, Schurch W, Gabbiani G. Smooth-muscle differentiation in stromal cells of malignant and non-malignant breast tissues. Int J Cancer 1988;41:707–712.
8. Miura S, Kodaira S, Hosoda Y. Immunohistologic analysis of the extracellular matrix components of the fibrous stroma of human colon cancer. J Surg Oncol 1993;53:36–42.
9. Neaud V, Faouzi S, Guirouilh J, Le Bail B, Balabaud C, Bioulac-Sage P, Rosenbaum J. Human hepatic myofibroblasts increase invasiveness of hepatocellular carcinoma cells: evidence for a role of hepatocyte growth factor. Hepatology 1997;26:1458–1466.
10. Doucet C, Jasmin C, Azzarone B. Unusual interleukin-4 and -13 signaling in human normal and tumor lung fibroblasts. Oncogene 2000;19: 5898–5905.
11. Lohr M, Schmidt C, Ringel J, Kluth M, Muller P, Nizze H, Jesnowski R. Transforming growth factor-beta1 induces desmoplasia in an experimental model of human pancreatic carcinoma. Cancer Res 2001;61: 550–555.
12. Rowley DR. What might a stromal response mean to prostate cancer progression? Cancer Metast Rev 1998;17:411–419.

13. Walter-Yohrling J, Pratt BM, Ledbetter S, Teicher BA. Myofibroblasts enable invasion of endothelial cells into three-dimensional tumor cell clusters: a novel in vitro tumor model. Cancer Chemother Pharmacol 2003;52:263–269.
14. Gilead A, Meir G, Neeman M. The role of angiogenesis, vascular maturation, regression and stroma infiltration in dormancy and growth of implanted MLS ovarian carcinoma spheroids. Int J Cancer 2004;108: 524–531.
15. Jain RK. Molecular regulation of vessel maturation. Nat Med 2003;9: 685–693.
16. Martin TA, Harding KG, Jiang WG. Regulation of angiogenesis and endothelial cell motility by matrix-bound fibroblasts. Angiogenesis 1999;3:69–76.
17. Kircher MF, Allport JR, Graves EE, Love V, Josephson L, Lichtman AH, Weissleder R. In vivo high resolution three-dimensional imaging of antigen-specific cytotoxic T-lymphocyte trafficking to tumors. Cancer Res 2003;63:6838–6846.
18. Modo M, Mellodew K, Cash D, Fraser SE, Meade TJ, Price J, Williams SC. Mapping transplanted stem cell migration after a stroke: a serial, in vivo magnetic resonance imaging study. Neuroimage 2004;21:311–317.
19. Huber MM, Staubli AB, Kustedjo K, Gray MH, Shih J, Fraser SE, Jacobs RE, Meade TJ. Fluorescently detectable magnetic resonance imaging agents. Bioconjug Chem 1998;9:242–249.
20. Bhorade R, Weissleder R, Nakakoshi T, Moore A, Tung CH. Macrocyclic chelators with paramagnetic cations are internalized into mammalian cells via a HIV-tat derived membrane translocation peptide. Bioconjug Chem 2000;11:301–305.
21. Kayyem JF, Kumar RM, Fraser SE, Meade TJ. Receptor-targeted cotransport of DNA and magnetic resonance contrast agents. Chem Biol 1995;2:615–620.
22. Gilad AA, Israely T, Dafni H, Meir G, Cohen B, Neeman M. Functional and molecular mapping of uncoupling between vascular permeability and loss of vascular maturation in ovarian carcinoma xenografts: the role of stroma cells in tumor angiogenesis. Int J Cancer 2005;117:202–211.
23. Dafni H, Israely T, Bhujwalla ZM, Benjamin LE, Neeman M. Overexpression of vascular endothelial growth factor 165 drives peritumor interstitial convection and induces lymphatic drain: magnetic resonance imaging, confocal microscopy, and histological tracking of triple-labeled albumin. Cancer Res 2002;62:6731–6739.
24. Silzle T, Kreutz M, Dobler MA, Brockhoff G, Knuechel R, Kunz-Schughart LA. Tumor-associated fibroblasts recruit blood monocytes into tumor tissue. Eur J Immunol 2003;33:1311–1320.
25. Borenfreund E, Puerner JA. Toxicity determined in vitro by morphological alterations and neutral red absorption. Toxicol Lett 1985;24: 119–124.
26. Razani B, Engelman JA, Wang XB, Schubert W, Zhang XL, Marks CB, Macaluso F, Russell RG, Li M, Pestell RG, Di Vizio D, Hou Jr H, Kneitz B, Lagaud G, Christ GJ, Edelmann W, Lisanti MP. Caveolin-1 null mice are viable but show evidence of hyperproliferative and vascular abnormalities. J Biol Chem 2001;276:38121–38138.
27. Stuart ES, Webley WC, Norkin LC. Lipid rafts, caveolae, caveolin-1, and entry by Chlamydiae into host cells. Exp Cell Res 2003;287:67–78.
28. Ferrucci JT, Stark DD. Iron oxide-enhanced MR imaging of the liver and spleen: review of the first 5 years. AJR Am J Roentgenol 1990;155:943–950.
29. Ahrens ET, Feili-Hariri M, Xu H, Genove G, Morel PA. Receptor-mediated endocytosis of iron-oxide particles provides efficient labeling of dendritic cells for in vivo MR imaging. Magn Reson Med 2003;49: 1006–1013.
30. Hinds KA, Hill JM, Shapiro EM, Laukkanen MO, Silva AC, Combs CA, Varney TR, Balaban RS, Koretsky AP, Dunbar CE. Highly efficient endosomal labeling of progenitor and stem cells with large magnetic particles allows magnetic resonance imaging of single cells. Blood 2003;102:867–872.
31. Bulte JW, Duncan ID, Frank JA. In vivo magnetic resonance tracking of magnetically labeled cells after transplantation. J Cereb Blood Flow Metab 2002;22:899–907.
32. Moore A, Sun PZ, Cory D, Hogemann D, Weissleder R, Lipes MA. MRI of insulitis in autoimmune diabetes. Magn Reson Med 2002;47:751–758.
33. Foster-Gareau P, Heyn C, Alejski A, Rutt BK. Imaging single mammalian cells with a 1.5 T clinical MRI scanner. Magn Reson Med 2003;49: 968–971.
34. Weissleder R, Elizondo G, Josephson L, Compton CC, Fretz CJ, Stark DD, Ferrucci JT. Experimental lymph node metastases: enhanced detection with MR lymphography. Radiology 1989;171:835–839.
35. Dousset V, Delalande C, Ballarino L, Quesson B, Seilhan D, Coussemacq M, Thiaudiere E, Brochet B, Canioni P, Caille JM. In vivo macrophage activity imaging in the central nervous system detected by magnetic resonance. Magn Reson Med 1999;41:329–333.
36. Kobayashi H, Kawamoto S, Saga T, Sato N, Ishimori T, Konishi J, Ono K, Togashi K, Brechbiel MW. Avidin-dendrimer-(1B4M-Gd)(254): a tumor-targeting therapeutic agent for gadolinium neutron capture therapy of intraperitoneal disseminated tumor which can be monitored by MRI. Bioconjug Chem 2001;12:587–593.
37. Geninatti Crich S, Barge A, Battistini E, Cabella C, Coluccia S, Longo D, Mainero V, Tarone G, Aime S. Magnetic resonance imaging visualization of targeted cells by the internalization of supramolecular adducts formed between avidin and biotinylated Gd(3+) chelates. J Biol Inorg Chem 2005;10:78–86.